Figure S1. Interferometric network for descending track T153. Red circle indicates the master image.
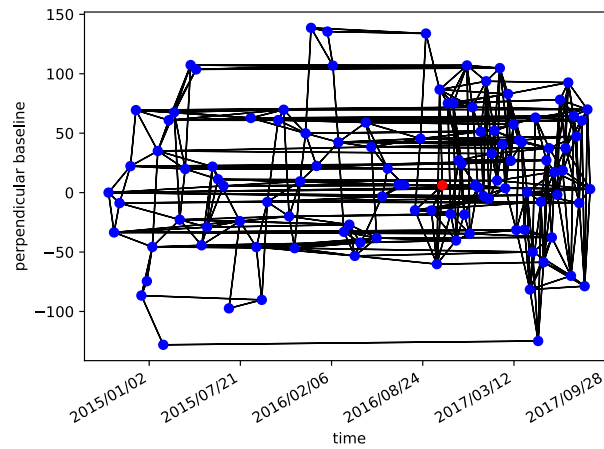
Figure S2. Interferometric network for ascending track T175. Red circle indicates the master image.
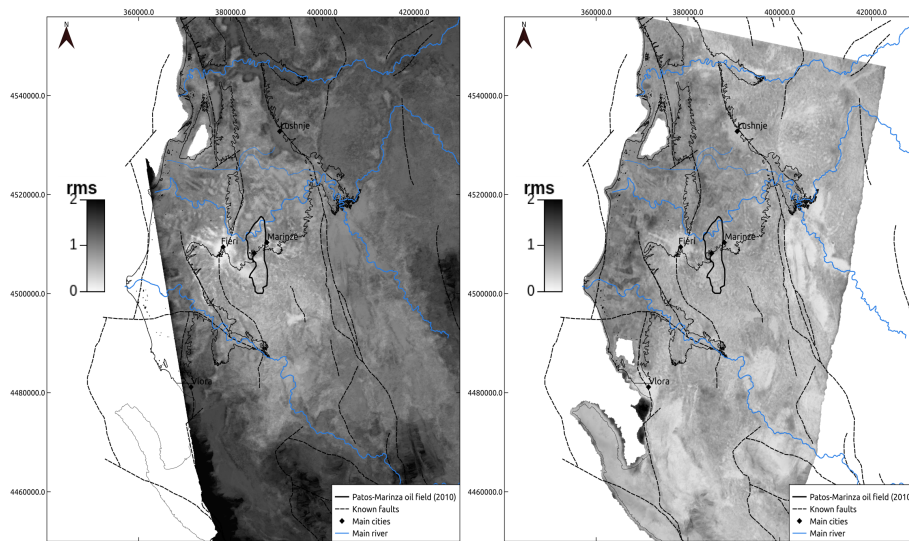
Figure S3. Large-scale view of the root mean square value by pixel for the ascending (left) and descending (right) tracks, given in radian. Reference areas for interferograms are chosen near Fieri (40.71°N,19.56°E) and Berat (40.73°N,19.93°E) cities, respectively.
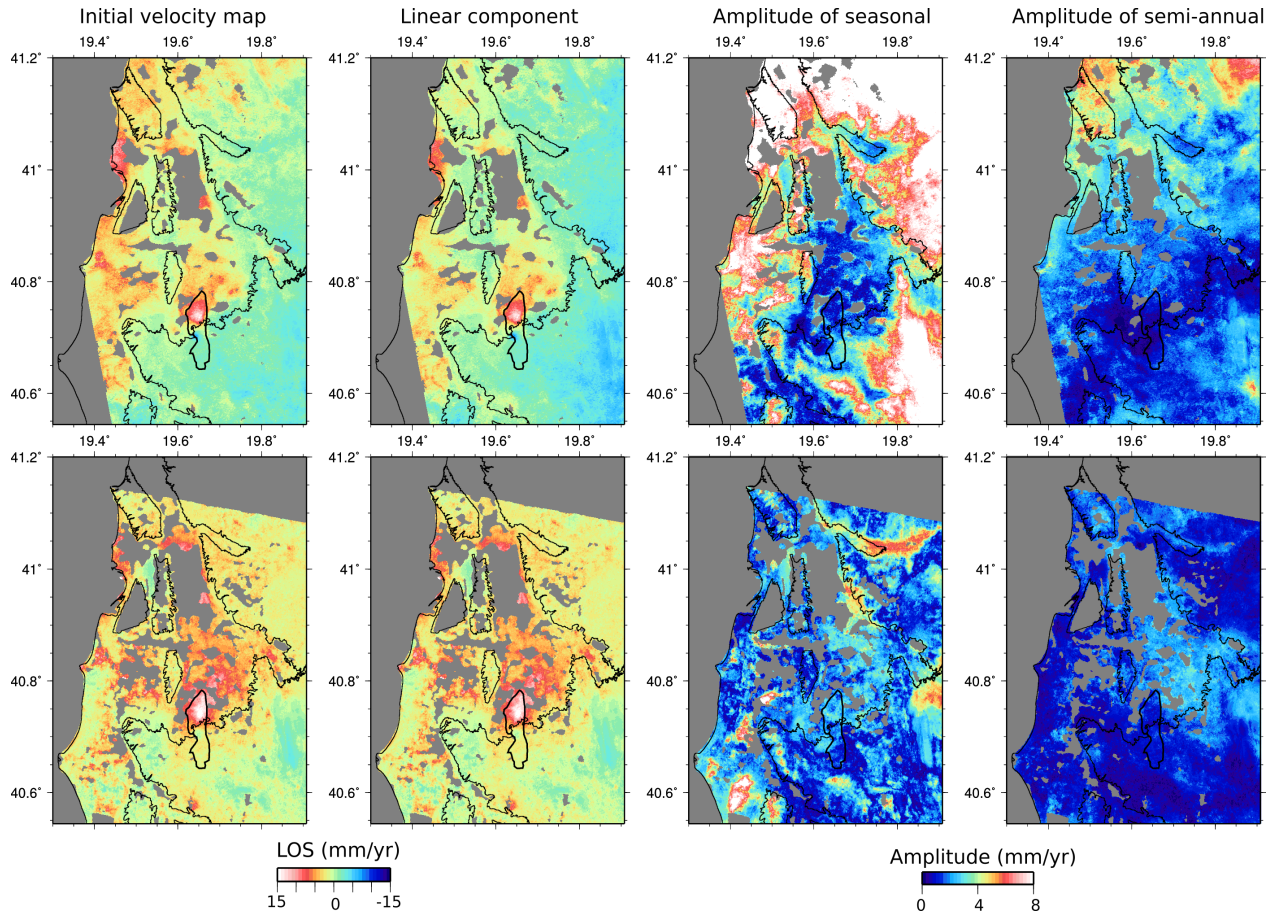
Figure S4. Decomposition of the estimated average velocity map (left) in linear plus annual and semiannual sinusoidal terms for ascending (top) and descending (bottom) tracks. The amplitude $\sqrt{(a^2 + b^2)}$ is plotted for the annual ($T = 1$yr) and semiannual ($T = 0.5$yr) terms in mm/yr, with velocity being $a.cos(2\pi t/T) + b.cos(2\pi t/T)$.
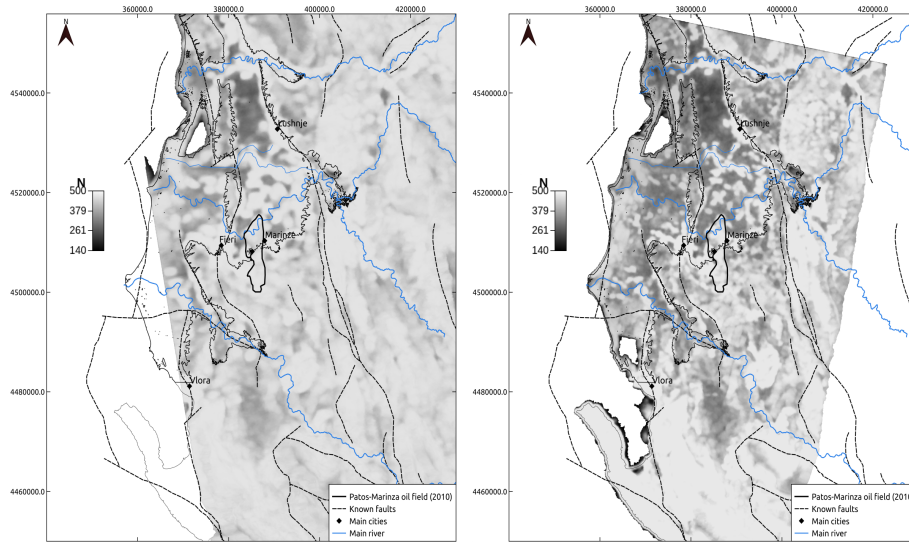
Figure S5. Large-scale view of the number of interferograms by pixel used in the time-series analysis to estimate the average velocity for the ascending (left) and descending (right) tracks. Based on these maps, we choose to discard pixels with less than 370 interferograms (∼75% of the total interferograms) to avoid poorly constrained average velocities.
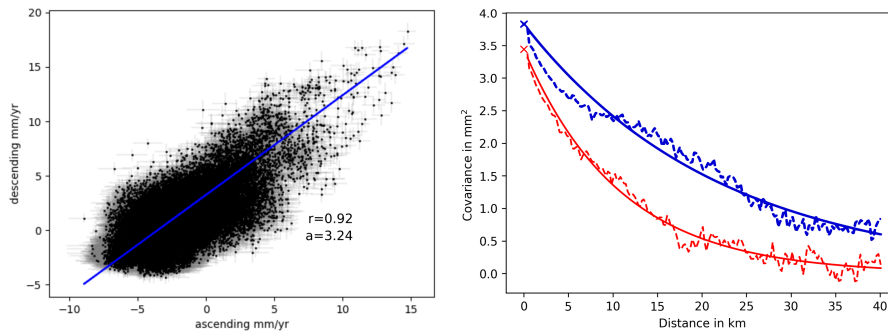
Figure S6. Left: Descending versus ascending LOS velocities for each pixel after masking based on Fig. S5. The very high correlation coefficient argues in favour of a consistent signal mainly due to vertical motion. The a value (given in mm/yr) is used as a constant to make both tracks consistent. Right: Covariograms of a stable portion of the ascending (red) and descending (blue) tracks (dashed curve), together with the best spherical model (plain curve). The covariance value for zero distance, equivalent to the overall variance of the image, is indicated as a red cross and differs by less than 0.5 mm^2 between both tracks. However, despite this similar variance, covariance is slightly higher at intermediate distances (10 to 20 km) for the descending track.